Journal of Power Sources 196 (2011) 4806–4810

Contents lists available at ScienceDirect

Journal of Power Sources

journal homepage: www.elsevier.com/locate/jpowsour

Short communication

Novel hedgehog-like 5 V $LiCoPO_4$ positive electrode material for rechargeable lithium battery

Fei Wang, Jun Yang*, Yanna NuLi, Jiulin Wang

School of Chemistry and Chemical Engineering, Shanghai Jiao Tong University, 800 Dongchuan Road, Shanghai, 200240, PR China

ARTICLE INFO

Article history:
Received 7 November 2010
Received in revised form 7 January 2011
Accepted 20 January 2011
Available online 26 January 2011

Keywords:
Lithium cobalt phosphate
Hedgehog-like
Solvothermal method
High voltage electrode
Lithium ion battery

ABSTRACT

Hedgehog-like $LiCoPO_4$ with hierarchical microstructures is first synthesized via a simple solvothermal process in water–benzyl alcohol mixed solvent at 200 °C. Morphology and crystalline structure of the samples are characterized by scanning electron microscope, transmission electron microscopy and X-ray diffraction. The hedgehog-like $LiCoPO_4$ microstructures in the size of about 5–8 μm are composed of large numbers of nanorods in diameter of ca. 40 nm and length of ca. 1 μm, which are coated with a carbon layer of ca. 8 nm in thickness by in situ carbonization of glucose during the solvothermal reaction. As a 5 V positive electrode material for rechargeable lithium battery, the hedgehog-like $LiCoPO_4$ delivers an initial discharge capacity of 136 mAh g^{-1} at 0.1 C rate and retains its 91% after 50 cycles, showing much better electrochemical performances than sub-micrometer $LiCoPO_4$ synthesized by conventional high-temperature solid-state reaction.

1. Introduction

Great attention has been paid to rechargeable lithium batteries as potential power sources for electric and hybrid electric vehicles because of the highest energy density of all the commercialized rechargeable batteries [1,2]. The positive electrode material with higher special capacities and higher voltage is a crucial factor to obtain higher battery energy density. In recent years, much work has focused on olivine-type $LiMPO_4$ (M = Fe, Mn, Co and Ni) and Nasicon-type $Li_3V_2(PO_4)_3$ as positive electrode materials owing to their low cost, high reversible capacity and good stability [3–6]. Although $Li_3V_2(PO_4)_3$ has large theoretical specific capacity, more than one voltage plateau involving in the process of charge and discharge may limit the practical application [7]. Among all these phosphates, $LiFePO_4$ has been widely investigated due to its advantages of long cycle life and reversibility [8–11]. However, the redox potential of Fe^{3+}/Fe^{2+} (3.5 V vs. Li/Li^+) is significantly lower than that of Mn^{3+}/Mn^{2+} (4.1 V vs. Li/Li^+), Co^{3+}/Co^{2+} (4.8 V vs. Li/Li^+), and Ni^{3+}/Ni^{2+} (>5.2 V vs. Li/Li^+) [12,13], resulting in its lower energy density compared to the other materials. In the case of $LiMnPO_4$ and $LiNiPO_4$, their extremely low electric conductivity (<10^{-10} S cm^{-1}) makes it difficult to exhibit Li^+ insertion/extraction [14,15]. Very recently, some significant breakthroughs have been achieved for $LiMnPO_4$ material by nanotechnology [16–18].

Owing to high operating potential close to 4.8 V vs. Li/Li^+ and relatively high theoretical specific capacity (167 mAh g^{-1}) [19], $LiCoPO_4$ is regarded as a promising 5 V electrode material for high-power batteries. However, the electrochemical performance of pristine $LiCoPO_4$ is very poor due to the low intrinsic electronic and ionic conductivity. Zhao et al. [20] prepared $LiCoPO_4$ microrods with the diameter of ca. 500 nm and length of ca. 5 μm by a hydrothermal method, which delivered a discharge capacity of only 65 mAh g^{-1} at 0.1 C. A progress in the reversible capacity and cyclability of $LiCoPO_4$ has been made by selective doping with cations and carbon coating. Han et al. [21] found that Fe doping could expand 1 D channel for Li^+ migration in polyanion structure of $LiCoPO_4$. Our group reported a vanadium doped $LiCoPO_4$ with a reversible capacity of about 135 mAh g^{-1} at 0.1 C [22]. Furthermore, vanadium doping leads to an enhancement of the discharge voltage plateau for about 70 mV. Carbon-coated $LiCoPO_4$ synthesized via microwave heating exhibited a discharge capacity of 144 mAh g^{-1} but the cyclability was still poor [23]. Wolfenstine et al. [24] reported that $LiCoPO_4$ containing 4–5 wt% Co_2P could deliver a capacity of 120 mAh g^{-1} at 0.2 C. The large discharge capacity was mainly due to the increased electronic conductivity, associated with the conductive Co_2P on the surface of $LiCoPO_4$ particles.

It is particularly significant to use nanoscaled particles for the $LiCoPO_4$ and other poly-anionic cathode materials with very low intrinsic electronic and ionic conductivity to enlarge the interfacial area of electrode/electrolyte and shorten the solid-state transport length of lithium ions. However, the nano-powders not only lead to low tap density, which reduces the volumetric energy den-

* Corresponding author. Tel.: +86 21 5474 7667; fax: +86 21 5474 7667.
E-mail address: yangj723@sjtu.edu.cn (J. Yang).

0378-7753/$ – see front matter © 2011 Elsevier B.V. All rights reserved.
doi:10.1016/j.jpowsour.2011.01.055

sity of the batteries, but also make troubles for the transport and electrode fabrication. Therefore, the ideal morphology for the poly-anionic cathode materials with high rate capability should contain microsized hierarchical architectures composed of nanosized building blocks such as nanopores, nanoparticles, nanorods and nanoplates. Herein, we first synthesize novel hedgehog-like $LiCoPO_4$ microstructures with numerous ordered nanorods by a facile solvothermal method at temperature as low as 200 °C without using any surfactant. Benefiting from this special complex micro-/nanoarchitectures, the obtained carbon-coated $LiCoPO_4$ shows good cyclic performance and rate capability.

2. Experimental

2.1. Sample synthesis

A solvothermal route was adopted to synthesize $LiCoPO_4$ samples and the effect of solvent on the $LiCoPO_4$ structure was explored. In a typical synthesis, the stoichiometric amounts of LiOH, $CoSO_4$ $7H_2O$, $(NH_4)_3PO_4$ $3H_2O$ and glucose (mole ratio is 3:1:1:0.5) were dissolved in 40 mL of mixed solvent containing water and benzyl alcohol (1:1 by volume). The concentration of Co^{2+} in the precursor was 0.1 mol L^{-1}. After vigorous stirring at room temperature for 20 min, the suspension was poured into a 50 mL Teflon-lined stainless steel autoclave. The sealed autoclave was heated in an oven at 200 °C for 8 h, and then cooled naturally. The product was filtered, washed with deionized water and absolute alcohol, and finally dried in air at 80 °C. To increase the electronic conductivity of carbon layer and obtain a highly crystalline olivine structure, the product power was calcined at 750 °C for 2 h in an argon atmosphere (denoted as $LiCoPO_4$−B). In addition, the sample was also prepared in pure water medium in the same process (denoted as $LiCoPO_4$−W). For a comparison, the $LiCoPO_4$/C composite was synthesized by conventional high-temperature solid-state reaction using Li_2CO_3, $Co(CH_3COO)_2$ $4H_2O$, $NH_4H_2PO_4$ and acetylene black. In short, the raw materials were ball-milled in ethanol, decomposed at 350 °C for 6 h and subsequently sintered at 750 °C for 12 h in flowing argon (denoted as $LiCoPO_4$−S).

2.2. Sample characterization

The crystalline phases of the samples were analyzed by X-ray diffraction (XRD) under a Rigaku D/Max-2200 diffractometer with Cu Kα radiation. The morphology and microstructure were observed using JEOL JSM-7401F scanning electron microscope (SEM) and transmission electron microscopy (TEM, JEOL JEM-2100). The carbon content was measured with PE 2400‖elemental analyzer.

2.3. Electrochemical measurements

The electrochemical tests were conducted with CR2016 cointype cells. The cathode was prepared by mixing 70 wt% active material, 20 wt% carbon black and 10 wt% polyvinylidene difluoride (PVDF) binder in N-methylpyrrolidone (NMP) solution. The homogeneous slurry was coated on aluminum foil and dried at 80 °C. The coated foil was punched into circular sheets of 12 mm in diameter, pressed at 5 MPa and further dried at 120 °C for 6 h in a vacuum oven. The cells were assembled in an argon-filled box, with lithium metal as anode and 1 M $LiPF_6$ in ethylene carbonate/dimethyl carbonate (1:1, v/v) as the electrolyte. Enter PE membrane served as a separator. Galvanostatic charge/discharge was carried out on a Land CT2001 battery test system between 3.2 and 5.1 V at 25 °C. Electrochemical impedance spectroscopic measurements (EIS) were performed with a Solartron SI 1287 electrochemical interface in the frequency range of 100 kHz–0.01 Hz with the amplitude of 5 mV.

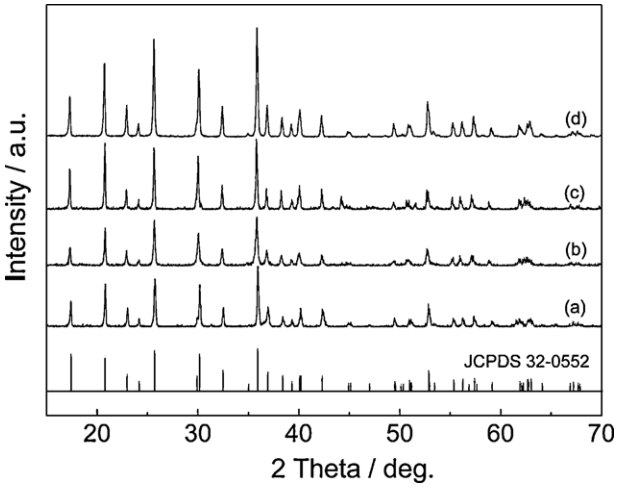

Fig. 1. XRD patterns of the $LiCoPO_4$ samples obtained from water–benzyl alcohol mixed solvent (a); from water (b); $LiCoPO_4$−B (c) and $LiCoPO_4$−S (d).

3. Results and discussion

3.1. XRD analysis

The XRD patterns of $LiCoPO_4$ samples obtained by different synthesis routes are shown in Fig. 1. The single olivine-type $LiCoPO_4$ with a *Pmnb* space group of orthorhombic system (JCPDS no. 32-0552) was obtained in water–benzyl alcohol mixed media (V/V = 1:1) when the reaction time exceeded 8 h (Fig. 1a). As exhibited in Fig. 1c, its diffraction peaks became much stronger after heat treatment at 750 °C, indicating the higher crystallinity of $LiCoPO_4$. In a parallel experiment, well crystallized $LiCoPO_4$ was also available after reaction for 8 h in pure water media (Fig. 1b). Fig. 1d shows the XRD patterns of $LiCoPO_4$ sample prepared by conventional high-temperature solid-state reaction. All the diffraction peeks correspond to pure $LiCoPO_4$ with olivine structure and no any impunity phases are observed. For all the samples, diffraction peaks of carbon cannot be detected due to its amorphous state or too low content.

3.2. SEM and TEM morphologies

Fig. 2 shows the SEM images of the samples obtained at different reaction times in water–benzyl alcohol mixed solvent. At the early stage of solvothermal reaction, the precursor nanoparticles gradually aggregated into microspheres as shown in Fig. 2a and b. With increasing the reaction time to 4 h, all the nanoparticles became regular microspheres with a diameter of 2–3 μm (Fig. 2c). As the reaction time lasted for 8 h (Fig. 2d), the microspheres evolved into hedgehog-like $LiCoPO_4$ hierarchical microstructure, where numerous ordered nanorods were self-assembled with a diameter of 35–50 nm and length of more than 1 μm. The higher magnification image of the nanorods is displayed in Fig. 2e. By contrast, the morphology of $LiCoPO_4$ prepared in water is littery and the width of prismatic $LiCoPO_4$ rods changes from 100 nm to near 1 μm (Fig. 2f). After annealing at 750 °C for 2 h, the original morphologies of $LiCoPO_4$−B microspheres and $LiCoPO_4$−W rods remained (Fig. 2g and h), indicating their good thermal stability. It is notable that such a hierarchical microstructure is not obtainable in our experiments replacing benzyl alcohol by other solvents miscible with water, such as ethanol, ethylene glycol and isopropanol. This

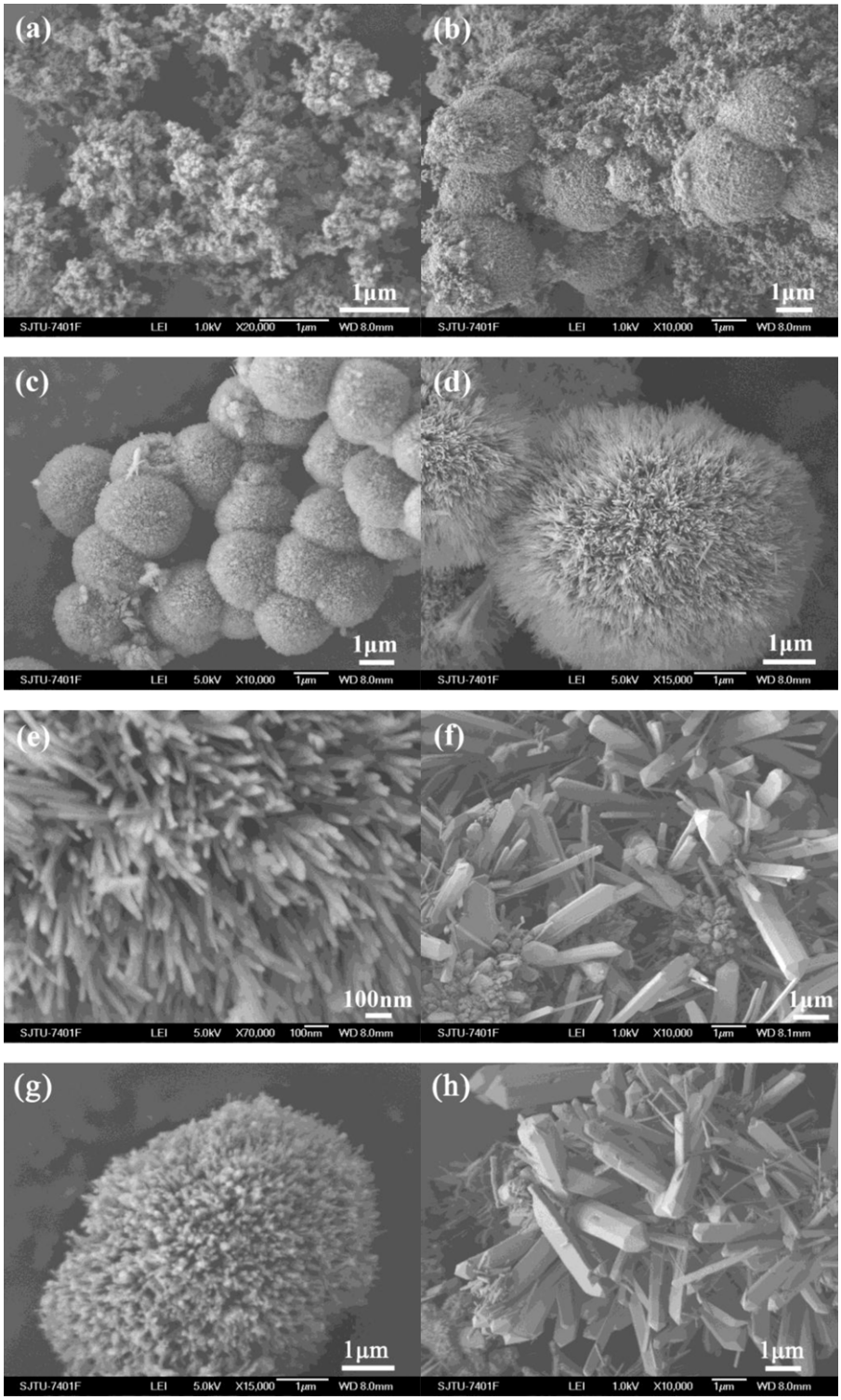

Fig. 2. SEM images of the $LiCoPO_4$ samples obtained from water–benzyl alcohol mixed solvent at different times: 0.5 h (a), 1 h (b), 4 h (c) and 8 h (dand e); from water: 8 h (f); after calcination: $LiCoPO_4$–B (g) and $LiCoPO_4$–W (h).

suggests that benzyl alcohol plays a crucial role in controlling the specific morphology and size. In view of that benzyl alcohol is difficult to be miscible with water due to its small solubility in water, the highly dispersed two-phase solvent system should be helpful for the morphology modulation under the conditions of high temperature and high pressure. The benzyl alcohol partially dissolved in water appears to act as a soft template or surfactant for the fabrication of the fine microstructure [25].

The TEM images of carbon-coated $LiCoPO_4$–S and $LiCoPO_4$–B are further compared in Fig. 3. For the $LiCoPO_4$–S in Fig. 3a, conductive carbon is well dispersed and forms a carbon network supplying the interconnection of sub-micrometer $LiCoPO_4$ particles. An inhomogeneous carbon layer with a thickness in ca. 20 nm is covered on the surface of $LiCoPO_4$ particles (Fig. 3b). Fig. 3c presents the morphology of hedgehog-like $LiCoPO_4$–B in diameter of 5–8 μm. The high-resolution TEM image of one nanorod from $LiCoPO_4$–B in

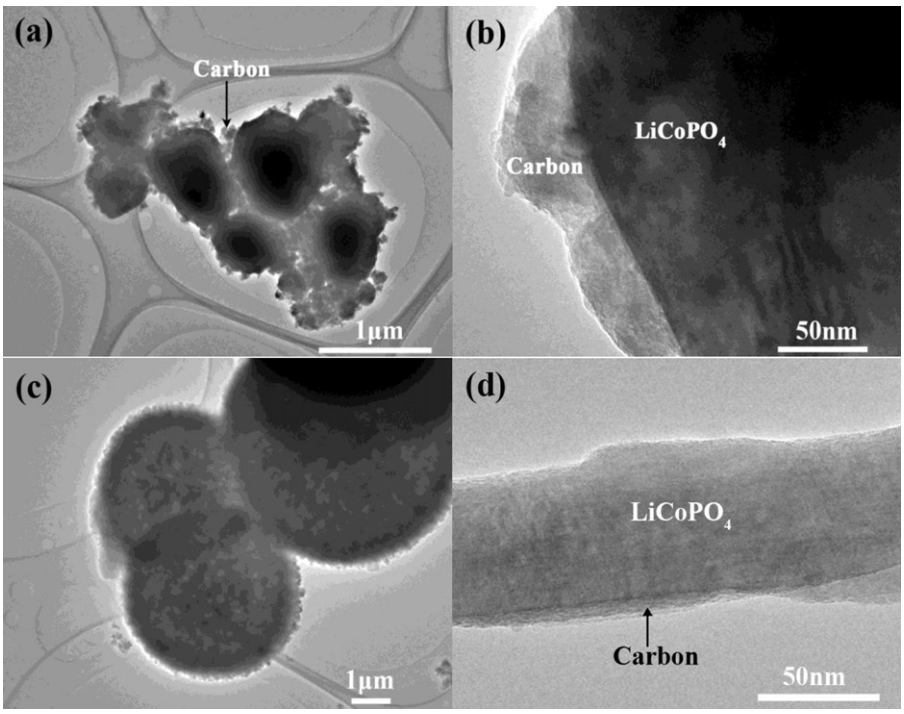

Fig. 3. TEM images of carbon-coated $LiCoPO_4$−S (a and b) and $LiCoPO_4$−B (c and d).

Fig. 3d reveals that it is encapsulated by a carbon layer mostly in a thickness of less than 10 nm, which is formed by in situ carbonization of glucose at 200 °C in the solvothermal process. Depending on elemental analysis, the amount of carbon in $LiCoPO_4$−S and $LiCoPO_4$−B is about 5.1 wt% and 3.4 wt%, respectively.

3.3. Electrochemical properties

Fig. 4 shows the typical (second) charge and discharge profiles of the different $LiCoPO_4$ electrodes at 0.1 C rate (16.7 mAh g^{-1}) in the voltage range from 3.2 V to 5.1 V. All the electrodes present a reversible voltage plateau around 4.8 V, corresponding to the redox couple of Co^{3+}/Co^{2+}. The discharge capacities of $LiCoPO_4$−B, $LiCoPO_4$−W and $LiCoPO_4$−S are 133, 90 and 109 mAh g^{-1}, respectively. It is worth noting that the $LiCoPO_4$−B electrode has a remarkably smaller hysteresis between charge and discharge voltage than the others. This low electrochemical polarization is ascribed to the morphology factor that the ordered nanorod structure facilitates the fast diffusion of lithium ions. Fig. 5 gives a comparison of the cyclic performance of the three electrodes. Besides the high discharge capacity, the $LiCoPO_4$-B also presents fairly good cyclic stability. After 50 cycles, 91% of the initial capacity of 136 mAh g^{-1} can be retained for the $LiCoPO_4$−B at 0.1 C rate. By contrast, the capacity of $LiCoPO_4$−W decreases from 93 mAh g^{-1} to 44 mAh g^{-1}. Its capacity retention is only 47%. Also the $LiCoPO_4$−B is absolutely superior to the conventional $LiCoPO_4$−S material in the specific capacity and cyclic stability.

Fig. 6 compares the discharge rate capability of $LiCoPO_4$−B and $LiCoPO_4$−S from 0.1 C to 5 C. In this test, the charge rate remains constant at 0.1 C along with increasing discharge rates. The $LiCoPO_4$−B exhibits superior rate performance compared to the $LiCoPO_4$−S. Discharge capacity of the $LiCoPO_4$−B can reach 85 mAh g^{-1} at 5 C, while its voltage plateau around 4.4 V remains distinct. The capacity retention at 5 C is 63% compared with the capacity at 0.1 C. Nevertheless, this value is only 42% for $LiCoPO_4$−S. In addition,

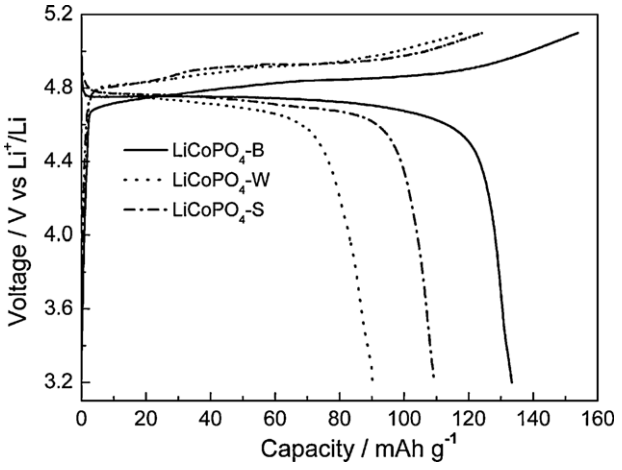

Fig. 4. The second charge/discharge profiles of $LiCoPO_4$−B, $LiCoPO_4$−W and $LiCoPO_4$−S at 0.1 C rate.

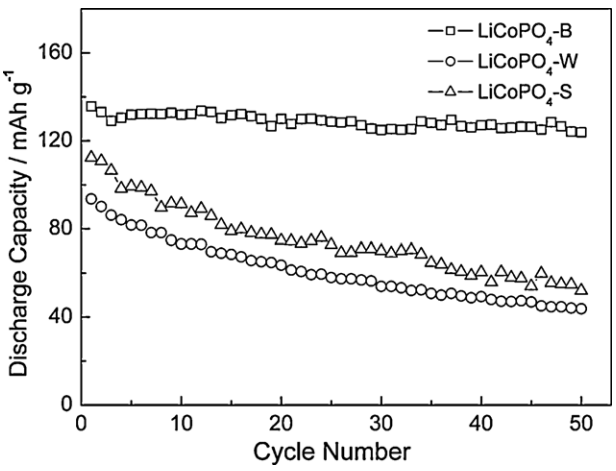

Fig. 5. Cycle performances of $LiCoPO_4$−B, $LiCoPO_4$−W and $LiCoPO_4$−S at 0.1 C rate.

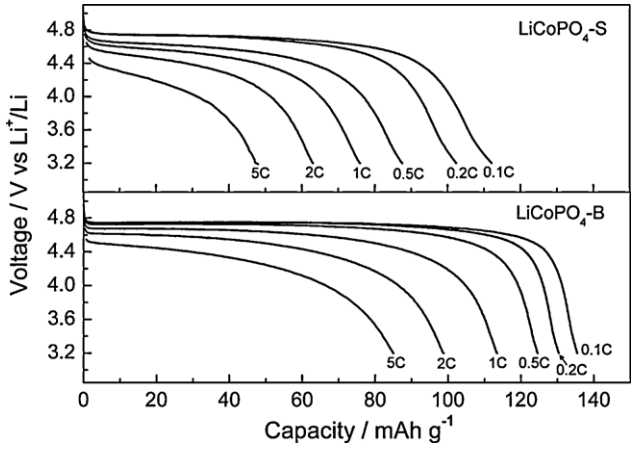

Fig. 6. Discharge curves of $LiCoPO_4$−S and $LiCoPO_4$−B at various discharge rates.

its discharge voltage and plateaus character noticeably turn down with increasing the current rate. The main reason for this big difference is the fact that the lithium ion diffusion depth of ca. 20 nm for the $LiCoPO_4$−B is much shorter than that of 200–400 nm for $LiCoPO_4$−S (see Fig. 3).

The interfacial reaction resistance and its change during cycling are further examined by electrochemical impedance spectroscopy (EIS) measurements. Fig. 7 shows Nyquist plots of the cells using $LiCoPO_4$−B and $LiCoPO_4$−S electrodes at the fully charged state after 1, 10, 30 and 50 cycles. All the spectra exhibit a semicircle in the high-frequency range and a sloping line in low-frequency range. The semicircle is assigned to the charge-transfer impedance of the electrochemical reaction, while the sloping line represents the Warburg impedance of lithium ion diffusion control. The diameter of the semicircle for Li/$LiCoPO_4$−S cell is significantly larger than that for Li/$LiCoPO_4$−B cell under the same cycle number. Smaller charge-transfer impedance of the $LiCoPO_4$−B is attributed to its larger specific surface area. Moreover, the semicircle augment of the $LiCoPO_4$−B with the progressive cycle number is not as marked as that of the $LiCoPO_4$−S. It means that the interfacial property of the $LiCoPO_4$−B is more stable during cycling, in accordance with the capacity stability in Fig. 5.

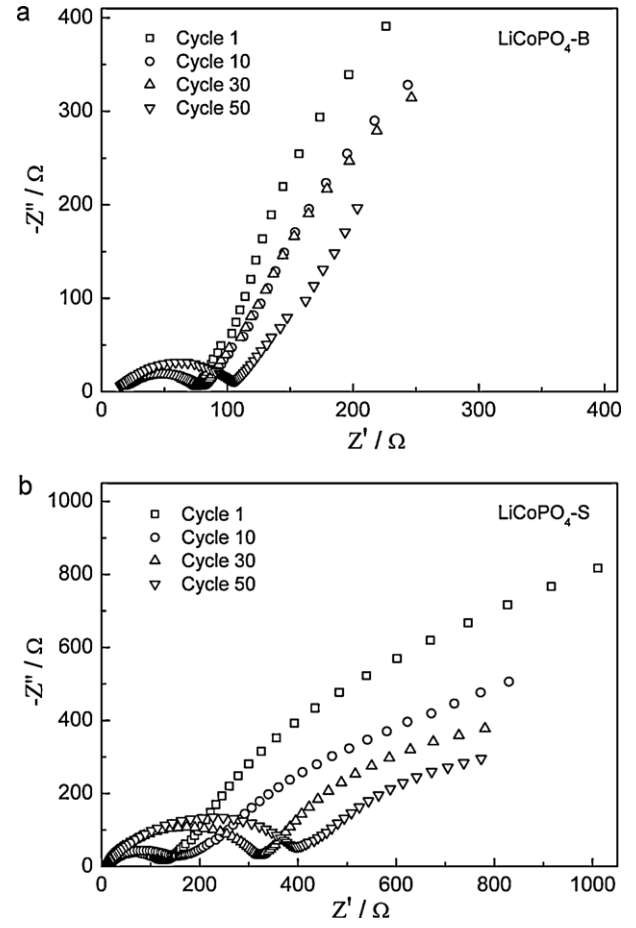

Fig. 7. Nyquist plots of the cells using $LiCoPO_4$−B and $LiCoPO_4$−S electrodes at the fully charged state at different cycling stages.

4. Conclusions

Hedgehog-like $LiCoPO_4$ microstructure material constructed by numerous carbon-coated nanorods was successfully prepared by solvothermal route in a mixed solvent of water and benzyl alcohol without using templates and surfactants. The presence of benzyl alcohol in water plays a key role in controlling the morphology and rod size of the product. This nanomicro structured $LiCoPO_4$ electrode material exhibits a relatively high specific capacity, superior capacity retention and rate performance. The significantly improved electrochemical performance can be mainly attributed to the enlarged interfacial area and shortened solid-state transport length of lithium ions. The facile approach reported herein may be extended to synthesize other nanomaterials with unique structural features.

Acknowledgement

This work was supported by National 973 Program (No. 2007CB209700).

References

[1] G. Ceder, Y.M. Chiang, D.R. Sadoway, M.K. Aydinol, Y.I. Jang, B. Huang, Nature 392 (1998) 694–696.
[2] A.M. Andersson, D.P. Abraham, R. Haasch, S. MacLaren, J. Liu, K. Amine, J. Electrochem. Soc. 149 (2002) A1358–A1369.
[3] H. Yang, X.L. Wu, M.H. Cao, Y.G. Guo, J. Phys. Chem. C 113 (2009) 3345–3351.
[4] C. Delacourt, P. Poizot, M. Morcrette, J.-M. Tarascon, C. Masquelier, Chem. Mater. 16 (2004) 93–99.
[5] C.A.J. Fisher, V.M.H. Prieto, M.S. Islam, Chem. Mater. 20 (2008) 5907–5915.
[6] M.M. Ren, Z. Zhou, X.P. Gao, W.X. Peng, J.P. Wei, J. Phys. Chem. C 112 (2008) 5689–5693.
[7] S.-C. Yin, H. Grondey, P. Strobel, M. Anne, L.F. Nazar, J. Am. Chem. Soc. 125 (2003) 10402–10411.
[8] Y.G. Wang, Y.R. Wang, E. Hosono, K.X. Wang, H. Zhou, Angew. Chem. Int. Ed. 47 (2008) 7461–7465.
[9] B. Kang, G. Ceder, Nature 458 (2009) 190–193.
[10] Y. Huang, H. Ren, S. Yin, Y. Wang, Z. Peng, Y. Zhou, J. Power Sources 195 (2010) 610–613.
[11] S. Yang, X. Zhou, J. Zhang, Z. Liu, J. Mater. Chem. 20 (2010) 8086–8091.
[12] A.K. Padhi, K.S. Nanjundaswamy, J.B. Goodenough, J. Electrochem. Soc. 144 (1997) 1188–1194.
[13] J. Wolfenstine, J. Allen, J. Power Sources 142 (2005) 389–390.
[14] C. Delacourt, L. Laffont, R. Bouchet, C. Wurm, J.B. Leriche, M. Morcette, J.M. Tarascon, C. Masquelier, J. Electrochem. Soc. 152 (2005) A913–A921.
[15] K. Rissouli, K. Benkhouja, J.R. Ramos-Barrado, C. Julien, Mater. Sci. Eng. B 98 (2003) 185–189.
[16] D. Wang, H. Buqa, M. Crouzet, G. Deghenghi, T. Drezen, I. Exnar, N.-H. Kwon, J.H. Miners, L. Poletto, M. Gratzel, J. Power Sources 189 (2009) 624–628.
[17] D. Choi, D. Wang, I.-T. Bae, J. Xiao, Z. Nie, W. Wang, V.V. Viswanathan, Y.J. Lee, J.-G. Zhang, G.L. Graff, Z. Yang, J. Liu, Nano Lett. 10 (2010) 2799–2805.
[18] Z. Bakenov, I. Taniguchi, Electrochem. Commun. 12 (2010) 75–78.
[19] K. Amine, H. Yasuda, M. Yamachi, Electrochem. Solid-State Lett. 3 (2000) 178–179.
[20] Y. Zhao, S. Wang, C. Zhao, D. Xia, Rare Met. 28 (2009) 117–121.
[21] D.-W. Han, Y.-M. Kang, R.-Z. Yin, M.-S. Song, H.-S. Kwon, Electrochem. Commun. 11 (2009) 137–140.
[22] F. Wang, J. Yang, Y. NuLi, J. Wang, J. Power Sources 195 (2010) 6884–6887.
[23] H.H. Li, J. Jin, J.P. Wei, Z. Zhou, J. Yan, Electrochem. Commun. 11 (2009) 95–98.
[24] J. Wolfenstine, J. Read, J.L. Allen, J. Power Sources 163 (2007) 1070–1073.
[25] Y.X. Zhou, H.B. Yao, Q. Zhang, J.Y. Gong, S.J. Liu, S.H. Yu, Inorg. Chem. 48 (2009) 1082–1090.